Equivalent circuit modelling of high-speed coplanar strip InP-based Mach-Zehnder phase modulators

J. A. Hillier, M. J. Wale, K. A. Williams, and W. Yao.

Eindhoven Hendrik Casimir Institute, Eindhoven University of Technology, Eindhoven, The Netherlands.

We explore the semi-analytical design strategies for indium phosphide (InP) based Mach-Zehnder modulators (MZMs), leveraging their superior electro-optic efficiency, lower intrinsic carrier concentration, and high thermal conductivity for high-bandwidth modulation. These modulators enable integrated photonics circuits with active and passive components on a single chip. High-performance, co-planar stripline MZMs on the generic InP platform have been shown allowing smaller device footprint and reduced microwave loss, maintaining high bandwidth and compatibility with generic foundry processes. We develop an analytical equivalent circuit model that facilitates swift extraction and optimisation of key performance metrics such as the electrical $-6\ dB$ *and electro-optic* -3 dB *bandwidths. This model is not only significantly more efficient than conventional finite element methods but also provides a physical intuition on the interrelationships between design parameters and enables wide-scale optimisation of the design geometry to produce bandwidths exceeding the current state-of-art (*$> 120\ GHz$*).*

Introduction

Advancements in design and manufacturing have propelled state-of-the-art InP-based Mach-Zehnder modulators (MZMs) to achieve impressive bandwidths of up to 80 GHz [1] alongside large data rates of ≥ 100 Gb/s by employing high-order modulation formats [2]. Future developments in fabrication and material enhancements promise to extend these bandwidths even further [3,4], though there is still room for design-only improvements to achieve bandwidths exceeding 100 GHz in MZMs. The most accurate methods for circuit design optimisation such as the semi-analytical method of lines [5] and finite difference methods [6] are often limited by their computational intensity, hindering a comprehensive design exploration. On the other hand, less computationally demanding methods typically depend on empirical approaches, fitting measured results to the lumped components of standard transmission line (TL) theory. Although these methods are useful for local optimisation [7], their validity is restricted to specific measurement conditions and fail to delve deeply into the physical principles that constrain MZM performance. To overcome these limitations, semi-analytical, non-iterative, and spatially resolved equivalent-circuit models have been developed for traveling-wave electrode MZMs [8]. These models compute the electronic propagation across the TL from the fundamental material and dimensional parameters of the modulator's structure, integrating both electronic and electro-optic (EO) behaviour. In this work, we apply the equivalent circuit modelling (ECM) approach to the novel co-planar strip (CPS) design that has recently demonstrated significantly enhanced performance over the traditional co-planar waveguide configuration [2]. We showcase the potential of this model through broad parameter exploration with elucidated effects on maximising the performance.

Equivalent circuit model

The Keysight Advanced Design System (ADS) environment was utilised to compute the propagation of electronic and optical signals along the phase shifter element. Integrated

EO analysis allows for the resultant phase and intensity modulation to be optimisable parameters, directly from the foundational material and device design properties. The model incorporates velocity matching, electrical reflections, and the influence of bias-voltage and temperature. **Figure 1** presents a schematic diagram for the cross section of the design. The phase modulator of length l_{ps} uses the CPS-TL geometry [2], comprising two parallel electrodes (gold-shaded layers in Figure 1) of width w_{sig} situated above a pair of waveguide stacks of width w_{wvg} separated by a distance g_{w2w} in such a way metal edge extends into the waveguide gap by a width g_{w2s} resulting in a gap between signal tracks with a width of $g_{s2s} = g_{w2w} - g_{w2s}$. For each waveguide stack, an unintentionally doped 'intrinsic' InP waveguide layer (white layer) is sandwiched between a 'p-cladding' and 'n-cladding' layer (light green and light blue, respectively). A layer of InGaAs (dark green) is utilised as a 'p-contact' layer between the p-cladding and signal track. The ground tracks lie on top of an 'n-bottom' layer (dark blue) to allow for a positive voltage applied to an 'n-metal' pad to provide a shared negative voltage (in y-direction) across the two waveguides. This enables the voltage to be shifted to the quadrature point of the MZM. A polyimide passivation layer (pink layer) exists between the electrodes. Each layer, $_L$, is described by a complex refractive index, $\widetilde{n_L} = n_L + j\kappa_L$, conductivity, σ_L, and thickness, d_L. The initial, pre-optimised, input parameters were taken from [3] and are not fit to any data. A single segment of the circuit model for the electrode is overlaid onto the schematic cross-section in Figure 1. The circuit is divided into $N = 30$ sections of length Δz and the electronic transfer mechanisms are denoted by discrete lumped components within each segment of the phase shifter. The frequency dependent values of impedance, L, complex inductance, $\tilde{Z}$, conductance, G, and capacitance, C, for each lumped component in Figure 1 are derived for the CPS design.

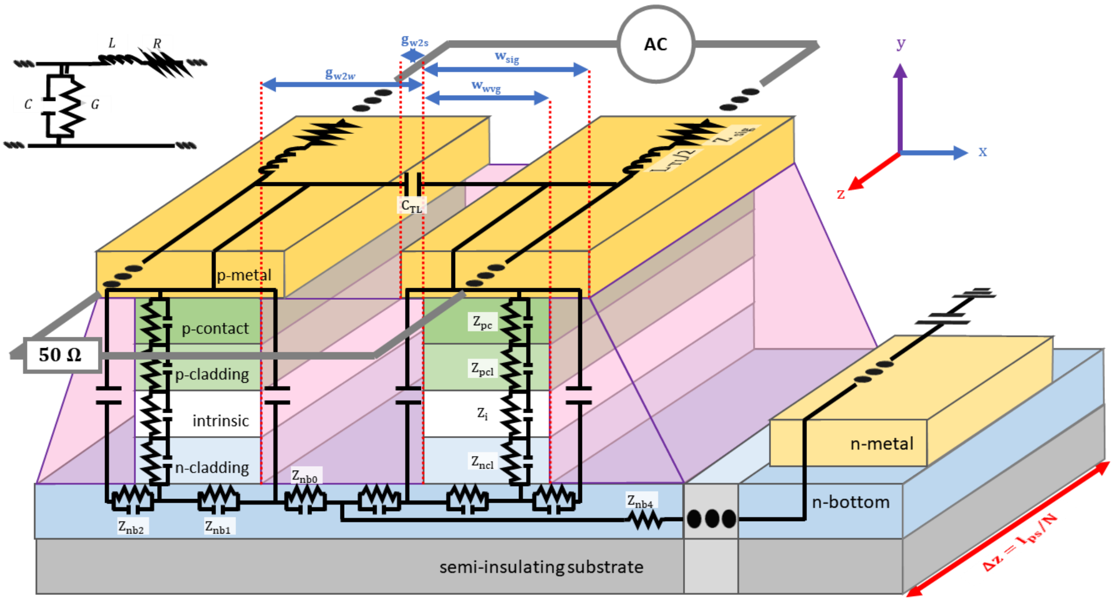

Figure 1. Schematic diagram of the electrical equivalent circuit used in the analytical simulations (black lines), showing one 'segment' of 30 within the phase shifter chain, including the corresponding lumped component parameters (black labels), as well as the out of plane electrical AC and DC voltage sources and the 50 Ω termination (grey lines). The circuit diagram is overlaid onto an illustration of the phase modulator element showing the material type and for each layer, the design dimensions (blue and red arrows).

The waveguide stack and polyimide layer capacitance and conductance are calculated from the permittivity and conductivity, respectively, using the ratio of the cross-sectional area to path length [9]. The complex impedance for each electrode is defined as the ratio of the metal layer skin depth resistivity to the electrode width [10]. The CPS-TL inductance through air is calculated using the conformal mapping [11], with a geometric moduli offered by the device geometry [12]. Substrate capacitance and conductance are assumed to be negligible. We also account for temperature and bias voltage influences on the depletion layer thickness [13] and intrinsic layer conductivity [9]. The microwave velocity is given by $v_\mu = \mathrm{Re}(L_{eff}C_{eff})^{-1/2}$, where the effective values of inductance of capacitance are calculated following a series of steps incorporating Kirchhoff's laws to reduce the complex circuitry to the form of a simple TL (inset to the top-left of Figure 1). S-parameters are simulated for a two-port configuration. The -6 dB electrical bandwidth, BW_{EE}, is obtained from S21. Subsequently, the source termination was replaced with an AC voltage source ($|V_{AC}| = -5$ dBm) in order to compute the time and frequency dependent voltage across the intrinsic layer, $\widetilde{V}_{i,s}$, for each segment 's'. The velocity mismatch of the electronic and optical waves is accounted for by applying a phase shift to the electronic signal that results in the voltage across the intrinsic layer experienced by the propagating optical mode:

$$\widetilde{V}^*_{i,s} = \widetilde{V}_{i,s} \exp\left(\frac{2\pi j}{\lambda_0}(n_g - n_\mu)z\right) \ , \qquad (1)$$

where $n_g = 3.7$ and $\lambda_0 = 1550$ nm are the optical group index and wavelength [3], respectively. The cumulative phase modulation, $\Delta\phi$, is then given by:

$$\Delta\phi = \frac{n_g^3 \Delta z}{\lambda_0} \sum_s^N (r_{Pockels}|E_s^*| + r_{Kerr}|E_s^*|^2) \ , \qquad (2)$$

where $E_s = V_i/d_i$ is the electric field affecting the optical mode. $r_{Pock} = 1.4 \times 10^{-12}$ mV^{-1} and $r_{Pock} = 8.0 \times 10^{-21}$ mV^{-1} are the Pockels and Kerr coefficients for bulk InP [14]. Computing the effect of the phase shift on the output power gives the small-signal response [9] from which we calculate the -3 dB EO bandwidth, BW_{EO}. Vitally, all calculations are incorporated within the ADS environment, allowing for parameter sweeping and optimisation of any key performance metrics from the fundamental material properties and design parameters.

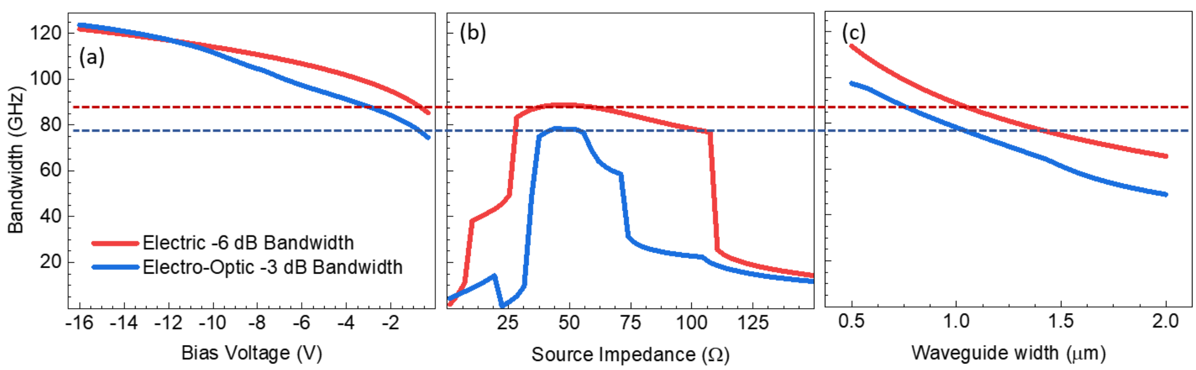

Figure 2. Electrical -6 dB and electro-optic -3 dB bandwidths as a function of (a) an applied bias voltage ($-16 - 0$ V), (b) the source/load impedance ($1 - 150\ \Omega$), and (c) the waveguide width ($0.5 - 2.0$ μm). The horizontal dashed red and blue lines indicate the electrical and electro-optic bandwidths, respectively, for the 'default' configuration.

Design space exploration

ECM simulations were ran for each design variable combination of 201 frequency steps and 50 parameter variations. Two independent simulations are required (EE and EO), totalling $20{,}100$ discrete simulations performed within $50\ \mathrm{s}$ ($\times\,3000$ improvement on computational time compared to finite element methods with comparable computational power [15]). Vitally, this enables an exploration of more variables using smaller increments and/or larger ranges within realistic time scales. To demonstrate this concept, Figure 2 presents $\mathrm{BW_{EE}}$ and $\mathrm{BW_{EO}}$ for variations in an indicative set of design parameters. Specifically, for variations in the (a) applied bias voltage, $\mathrm{V_{DC}}$, (b) source/load impedance, and (c) waveguide width. Figure 2a shows that both $\mathrm{BW_{EE}}$ and $\mathrm{BW_{EO}}$ increase by ~ 20 GHz as when $\mathrm{V_{DC}} = -6\ \mathrm{V}$, the quadrature point for fabricated MZMs with 1 mm long electrodes [2]. This bandwidth increase primarily arises from the increase in the depletion width of the p-n junction. This is modelled as an increases in the intrinsic layer thickness, reducing the capacitance across the intrinsic layer and subsequently the increasing the electric field and cumulative phase shift. This highlights the importance of considering all underlying physical phenomena, such as the depletion width dependence on voltage, within the modelling. It should be noted that, currently, the model does not factor in how the overlap integral between the electrical field and the optical mode may also change with increasing the depletion zone thickness. This may lead to reduced bandwidths for smaller values of $\mathrm{V_{DC}}$. Another important consideration is that $\mathrm{V_\pi}$ depends on the intrinsic layer thickness and thus on $\mathrm{V_{DC}}$. Therefore, $\mathrm{BW_{EO}/V_\pi}$, a ‘figure of merit’ for MZMs [15], is reduced from $23.2\ \mathrm{GHz/V}$ at $0\ \mathrm{V}$ to $20.7\ \mathrm{GHz/V}$ at $-6\ \mathrm{V}$. This highlights how $\mathrm{V_{DC}}$ must be carefully applied to optimise performance, especially for large signal measurements with under-driven modulators [2]. It is seen in Figure 2b that there exist a strong and complex dependence of $\mathrm{BW_{EE}}$ and $\mathrm{BW_{EO}}$ on the source and load impedances. This can be ascribed to the influence of back-reflections from the load especially at frequencies close to the bandwidth, due to impedance mismatch between the load and the TL. The characteristic impedance of the TL, $\mathrm{Z_{0,TL}}$, can be estimated from the equivalent circuit model to be $\sim 46\ \Omega$ at 85 GHz and $\mathrm{V_{DC}} = 0$. The peak in bandwidth occurs when there is a close match of the source and load impedances to $\mathrm{Z_{0,TL}}$. The sharp drops in $\mathrm{BW_{EO}}$ occur due to regions where the interference fringes in the frequency response cause the response to be relatively flat around -3 dB. Vitally, such fine details of the curve are possible to resolve in realistic time frames due to the semi-analytical model, allowing one to more accurately predict tolerances. In Figure 2c it is observed that reductions in the waveguide width can also enhance both $\mathrm{BW_{EE}}$ and $\mathrm{BW_{EO}}$. Such gains don’t affect $\mathrm{V_\pi}$ and so are more desirable than increasing the intrinsic layer thickness (either during fabrication or by increasing $\mathrm{V_{DC}}$). It should be noted that, there are presently technological limitations for reducing the waveguide width down to $0.5\ \mu\mathrm{m}$ [3].

Conclusions

We present an analytical, non-iterative, and spatially resolved equivalent circuit model for an EO-MZM using the CPS-TL configuration. The model takes only geometrical and material parameters as inputs, better elucidating the physical mechanisms behind device optimisation than both finite-difference and empirical circuit models as well as enabling fast and wide-range performance optimisation.

References

[1] A. Meighan, M. J. Wale, and K. A. Williams, "High-Density Coplanar Strip-Line Mach-Zehnder Modulators in a InP Generic Platform," European Conference on Optical Communication, 2021.

[2] J. A. Hillier, A. Meighan, M. Van Den Hout, S. Van Der Heide, S. Cakmakyapan, W. Yao, R. Van Dommele, M. Wale, C. Okonkwo, and K. Williams, "A 100 GBaud co-planar stripline Mach-Zehnder modulator on Indium Phosphide platform," Opto-Electronics and Communications Conference, 2023.

[3] W. Yao, "Towards a High-Capacity Multi-Channel Transmitter in Generic Photonic Integration Technology," Thesis, Eindhoven University of Technology, 2016.

[4] L. Thylén and L. Wosinski, "Integrated photonics in the 21st century," Photonics Res 2(2), 75 (2014).

[5] U. Rogge and R. Pregla, "Method of Lines for the Analysis of Strip-Loaded Optical Waveguides", Journal of. Optical Society America B, 8(2) (1991).

[6] J. Witzens, T. Baehr-Jones, and M. Hochberg, "Design of transmission line driven slot waveguide Mach-Zehnder interferometers and application to analog optical links," Optics Express 18, 16902 (2010).

[7] W. Yao, G. Gilardi, M. K. Smit, and M. J. Wale, "Equivalent circuit modelling of integrated traveling-wave optical modulator in InP foundry platform," 18th European Conference on Integrated Optics, 2016.

[8] H. Yu and W. Bogaerts, "An equivalent circuit model of the traveling wave electrode for carrier-depletion-based silicon optical modulators," Journal of Lightwave Technology 30, 1602–1609 (2012).

[9] G. Ghione, Semiconductor Devices for High-Speed Optoelectronics (Cambridge University Press, 2009).

[10] K. S. Giboney, "Travelling-Wave Photodetectors," Thesis, University of California (1995).

[11] Y. R. Kwon, V. M. Hietala, and K. S. Champlin, "Quasi-Tem Analysis of "Slow-Wave" Mode Propagation on Coplanar Microstructure Mis Transmission Lines," IEEE Trans Microw Theory Tech 35, 545–551 (1987).

[12] E. Chen and S. Y. Chou, "Characteristics of Coplanar Transmission Lines on Multilayer Substrates: Modeling and Experiments" IEEE Transactions on Microwave Theory and Techniques (1997), 45(6).

[13] S. M. Sze and K. K. Ng, *Physics of Semiconductor Devices*, John Wiley & Sons, Inc., 2006.

[14] S. Adachi, *Properties of Group-IV, III-V and II-VI Semiconductors*, John Wiley & Sons, Ltd, 2005.

[15] A. Meighan, "Co-design of the high-speed photonic and electronic integrated circuits", Thesis, Eindhoven University of Technology, 2021.